Predicting hydraulically-induced microseismic fractures from seismic inversion volumes: A North Texas Barnett Shale case study

Xavier E. Refunjol, University of Oklahoma, Joël Le Calvez, Schlumberger, Kurt J. Marfurt, and Katie M. Keranen, University of Oklahoma*

Summary

It is well-established that microseismic events induced by hydraulic stimulation are controlled by the present day stress field and preferentially open zones of weakness generated through structural deformation in the geologic past. In this paper, we show that the location of microseismic events measured in a survey acquired over Barnett Shale formation of the Fort Worth Basin also correlate to low P- and S-impedance volumes estimated from 3D surface seismic data. This correlation suggests that 3D surface seismic-derived attributes can serve as a tool in designing hydraulic stimulation programs. The ultimate objective is to optimize stimulation projects and thereby cost necessary to fully produce the resource by having *a priori* knowledge of most likely fracture propagation trends and where the formations will most likely fail.

Introduction

Hydraulic fracture stimulation is used to increase permeability and reactivate natural fractures (Williams-Stroud and Duncan, 2008; Eisner et al., 2010). Locating the sources of released energy from rock failure associated with hydraulic stimulation has shown preferential alignment with the maximum horizontal stress direction (Warpinski, 2004; Neale, 2010). Previous studies in the area of interest concluded that mapped microseismic development partially results from both the influence of the current stress regime and regional tectonic features. Gale et al. (2007) find that preferential orientation of the events mimic the presumed current horizontal maximum stress (NE-SW) as well as secondary perpendicular lineaments from secondary stress changes. These fracture-prone zones have shown evident relationship to volumetric curvature. Events occur away from the most negative curvature values, favoring areas in a small range of positive curvature values (Figure 1).

This investigation is based on a pre-stack time migrated seismic survey from North Texas Barnett Shale within the Fort Worth Basin acquired prior to any hydraulic stimulation. Four vertical wells with compressional and shear log measurements served as monitor wells for four corresponding horizontal Barnett Shale stimulation wells. The various gas-bearing formations of interest were hydraulically fractured along several intervals (or stages) in the horizontal part of the well.

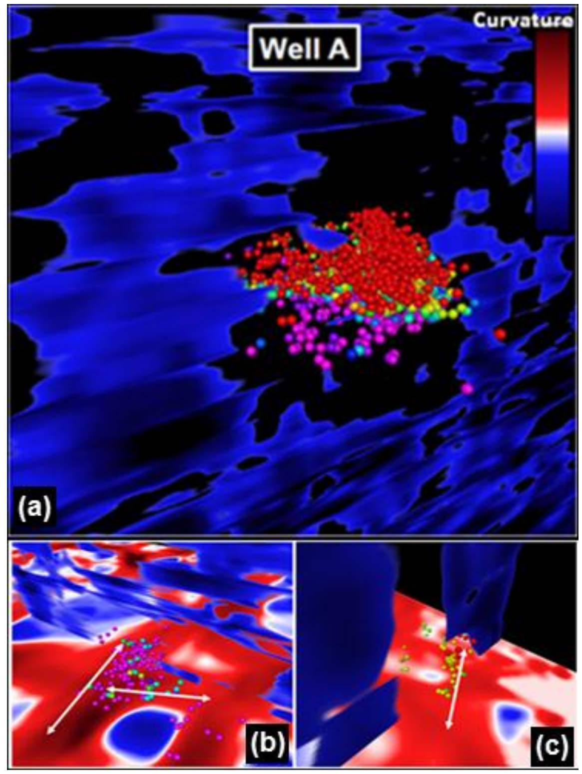

Figure 1. (a) Cross section of long wavelength most negative curvature vertical cross sections with a microseismic cloud. Events are mapped away from the most negative principal curvature. (b) and (c) Cross section of long wavelength most negative principal curvature with most positive curvature time slices through microseismic event clouds in the first and second hydraulic fracturing stages respectively.

Acoustic Impedance Inversion

To understand the relationship between mapped microseisms and the composition of the volumes where they occur we generated seismic P-impedance and S-impedance inversion volumes. Using a seismic survey acquired prior to stimulation presents an unaltered setting where common factors that led to the subsequent known failure foci can be observed and analyzed.

The inversion volumes (Figure 2) were generated using commercial model-based inversion algorithm based on density, sonic (P-wave), and dipole sonic (S-wave) logs from five wells within the study area, and high fold, wide-azimuth pre-stack seismic data gathers. The three assumptions made by the algorithm are that (i) the linearized approximation for reflectivity holds, (ii) reflectivity as a function of angle can be approximated by the Aki-Richards equations, and (iii) there is a linear relationship between P-impedance and both S-impedance and density.

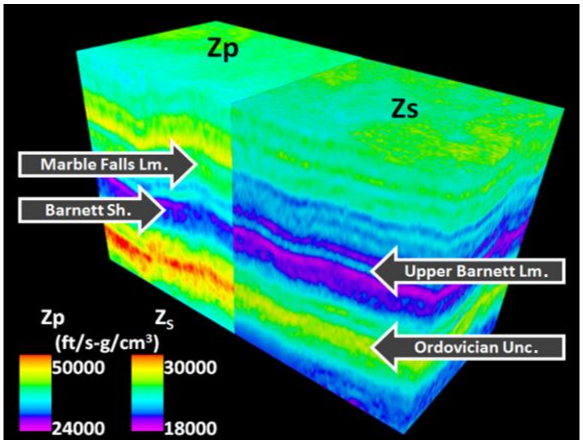

Figure 2. Cropped P-impedance and S-impedance volumes from seismic inversion with labeled formations.

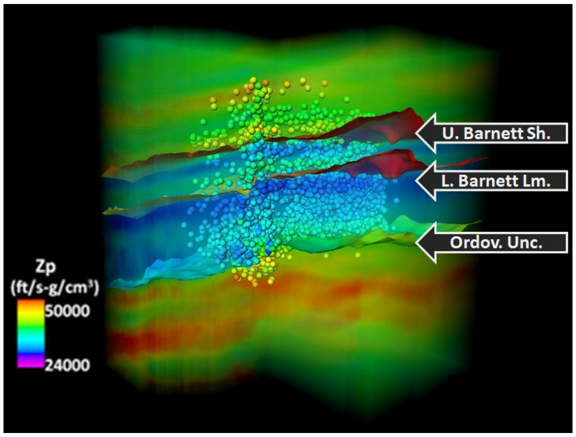

Figure 3. Microseismic events and surrounding inverted P-impedance volume. Events have been color coded with impedance values, mirroring the impedance color ranges from the impedance volume surrounding them. Surfaces help visualize the impedance changes between formations.

By design, the microseisms occur primarily within the formation being stimulated, in this case the Lower Barnett Shale. Locations of the microseismic events in the Barnett Shale have a good correlation to the inversion volumes, where they correspond to a narrow range of values for each property in all stimulation stages of the studied wells, regardless of their orientation and location.

Figure 3 provides a perspective view of the mapped microseismic event loci in the P-impedance volume. Horizons are indicated to confirm that most of the mapped activity develops within the treated interval of interest. To observe this in a quantitative manner, we plotted P-impedance and S-impedance histograms of the values corresponding to the microseisms against impedance values from the volume surrounding the stimulated area. The observed data suggest that fractures associated with hydraulic stimulation occur in lower impedance rock (Figure 4).

Furthermore, in wells where stimulation extended beyond the target formation, we find that fractures occur in the lower end of the impedance spectrum corresponding to each formation. For example, while the fractures in well A all occurred in the Lower Barnett Shale (Figure 4a) the stimulation of well B resulted in fracturing of the overlying Marble Falls Limestone, the target Barnett Shale, and the underlying Ordovician carbonates. In this well the bimodal behavior of the microseisms associated to the lower portions of the surrounding rock's bimodal impedance can be observed (Figure 4b). Since the fractured rocks are less dense than the surrounding areas and present lower impedance, a high velocity preferential occurrence can be inferred.

In order to further investigate this relationship, we generated P-impedance vs. S-impedance plots of the stimulated rock about the wells and those at the microseism locations. Figure 5 shows that there is greater occurrence of events for low values of Z_P and Z_S. Furthermore, events show a distinct linear trend corresponding to a value of Z_P/Z_S = 1.65. This crossplot suggests that we can use the inversion of surface seismic data to predict subsurface zones where the rock is more likely to fail and might serve as reservoir drainage pathways.

Our microseismic measurement based analysis shows that hydraulically stimulated rocks preferably fail within low impedance zones. All stages of all four fractured wells present the same behavior. This observation is in agreement with those of Rutledge and Phillips' (2003) who also find shear activation of fractures to be correlated to low-impedance. However, this observation contradicts the general assumption that hydraulic stimulation preferentially fractures brittle rock as it generates larger fracture systems and ultimately a more efficient drainage pathway (Grieser et al., 2007; Rickman et al., 2008). To reconcile these conflicting observations, we hypothesize that the low-impedance zones in our survey correspond to lower-impedance, calcite-cemented healed fractures that are more easily popped open than the undisturbed shale. Gale et al.

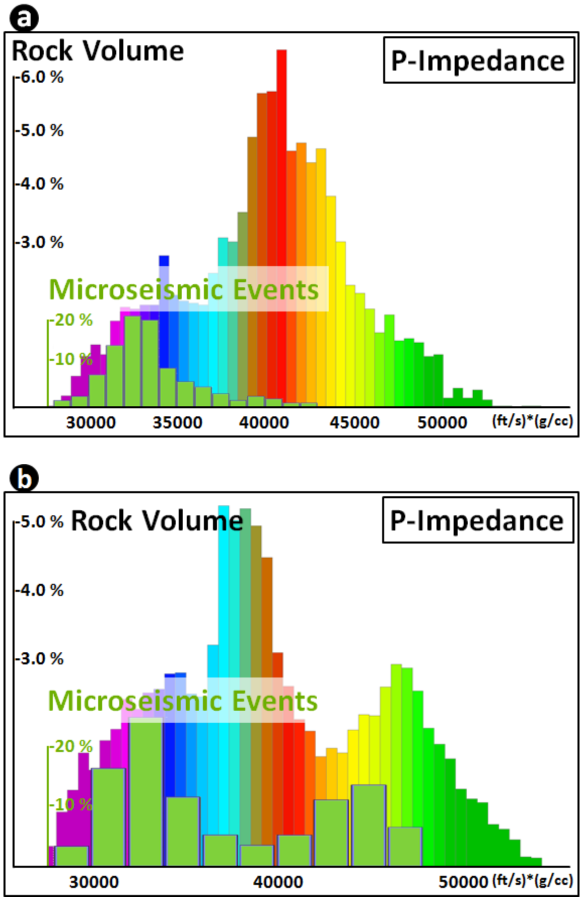

Figure 4. P-impedance values of the rock volume and of stimulated rock volume corresponding to microseismic event locations (in green) for (a) well A and (b) well B. (a) Note correlation of event location to lowest values of impedance in well A. (b) In contrast, well B exhibits a bimodal with the lower impedance events occurring within the Barnett Shale and higher impedance events in the overlying Marble Falls Limestone and underlying Ordovician carbonates.

(2007) have found that the tensile strength of the contact between the calcite fracture fill and the shale wall rock is low, leading to weak fracture-host boundary.

Similar to the impedance results, density histograms show preferential fracturing towards the lower end of the density spectrum. In other words, the observed events occur in the less dense areas of the rock volume (Figure 6). Taking into account the low impedance and low density character of the microseism-generating zones, the modulus could present high velocities. It is possible that while events might be occurring in lower density rock, they might have an asesimic behavior, or generate low non-recordable energy.

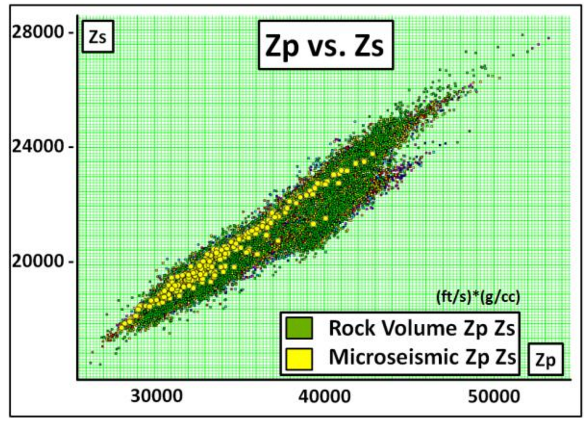

Figure 5. Cross plots of P- and S-impedance values of the rock volume (in green) and at the microseism event locations (in yellow).

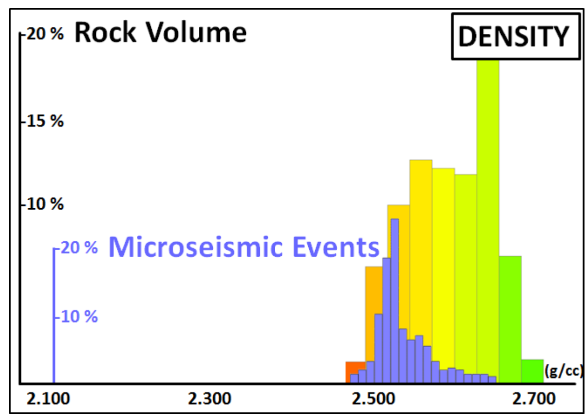

Figure 6. Density of stimulated rock volume and occurrence of microseisms for well A.

Lamé Parameters

We derived Lamé parameters λ and μ, incompressibility and rigidity respectively, from the acoustic impedances, using the relationship $\lambda\rho = Z_p^2 - 2Z_s^2$ and $\mu\rho = Z_s^2$, where ρ is the bulk density (Chopra and Pruden, 2003). These parameters have been used to improve delineation of reservoirs since incompressibility is more sensitive to the pore fluids than to the matrix, whereas the rigidity is influenced by the matrix connectivity only (Dufour et al., 2002). In Figure 7 we examine the relationship between Lamé parameters of microseism event location to the lambda-rho and mu-rho values of the surrounding rock.

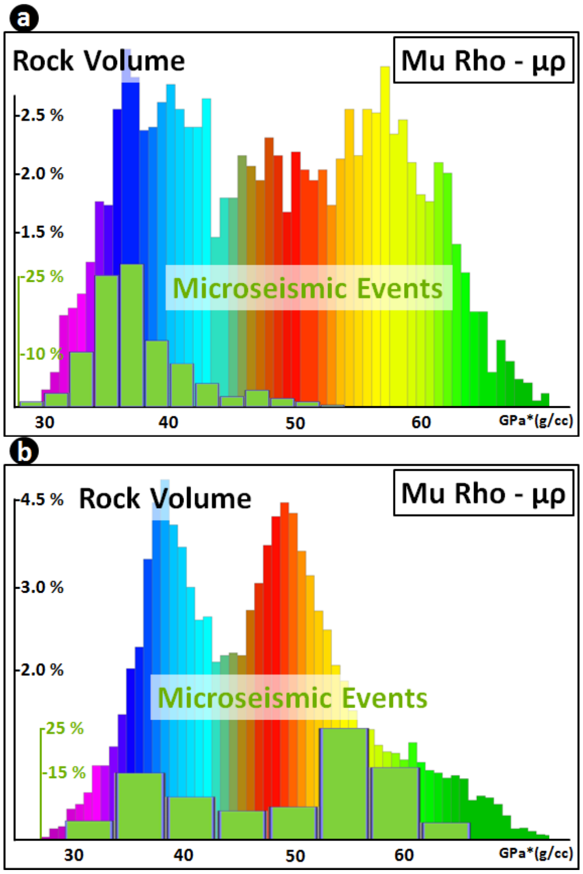

Figure 7. Histograms of microseismic $\mu\rho$ values compared to those of the surrounding volume of rock for (a) well A and (b) well B. (In well A events with low rigidity correspond to the Barnett Shale. In well B the bimodal distribution of microseismic rigidity values correspond to the low values of the Barnett Shale and the high values of Ordovician carbonates.

In well A we note a strong correlation to low incompressibility and rigidity values that correspond to those of the Barnett Shale. In well B where the stimulation reaches the Marble Falls Limestone and Ordovician carbonates we observe a bimodal behavior of the histogram, with the first mode corresponding to Barnett Shale values and the second mode corresponding to carbonate values. In these cases, the lowest LMR zones of the Barnett Shale mode remain fracture-prone, while the high values of the Ordovician Carbonates mode are the ones fractured (Figure 7b).

In Figure 8 we display a cross plot of $\lambda\rho$ vs. $\mu\rho$ in the surrounding rock (in green) and values at the microseism event locations (in yellow). We note a linear trend of the microseismic points, breaking into two subclusters, indicating the fractures in both the Barnett Shale and the Ordovician Carbonates (Figure 8).

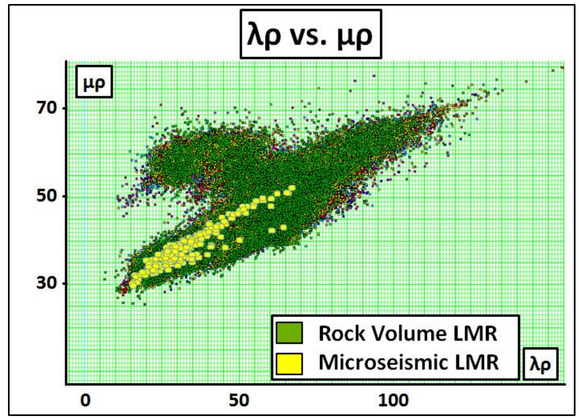

Figure 8. Cross plots of $\lambda\rho$ and $\mu\rho$ values of the rock volume (in green) and at the microseism event locations (in yellow).

Ideally, we need to augment our prediction tool to incorporate the correlations between microseismic events and curvature. Additional calibration of these correlations should allow to more accurately predict possible fracture zones as well as to lower risk, and to stimulate more effectively a given target zone.

Conclusions

We propose predicting fracture prone zones in the subsurface from prestack P- and S-impedance inversion of surface seismic data calibrated to microseismic event locations. Coupling this observation with the correlation of induced fractures with curvature anomalies, we anticipate a workflow that provides *a priori* knowledge of potential fracture system distribution. Such prediction can lead to increased recovery rates from a hydraulic stimulation with knowledge of possible drainage pathways that lead to target zones.

Acknowledgments

We thank Devon Energy for providing financial support, data and permission to publish this work. Thanks to Schlumberger and Hampson-Russell for providing licenses used in interpretation and inversion process respectively.

References

Chopra, S., and Pruden, D., 2003, Multiattribute seismic analysis on AVO-derived parameters - A case study: The Leading Edge, **10**, 998-1002.

Dufour, J., Squires, J., Goodway, W. N., Edmunds, A., and I. Shook, 2002, Integrated geological and geophysical interpretation case study, and Lamé rock parameter extractions using AVO analysis on the Blackfoot 3C-3D seismic data, southern Alberta, Canada: Geophysics, **67**, 27-37.

Eisner, L., Williams-Stroud, S., Hill, A., Duncan, P., and M. Thornton, 2010, Beyond the dots in the box: Microseismicity-constrained fracture models for reservoir simulation: The Leading Edge, **29**, 326.

Gale, J. F., Reed, R. M, and J. Holder, 2007, Natural fractures in the Barnett Shale and their Importance for hydraulic fracture treatments: AAPG Bulletin, **91**, 603-622.

Grieser, B., and Bray, J., 2007, Identification of production potential in unconventional reservoirs: Presented at the Production and Operations Symposium, SPE.

Neale C., 2010, Cost-effective, high-resolution hydraulic fracture microseismic monitoring – anywhere, anytime: E&P, **83**, 46-48.

Rickman, R., Mullen, M., Petre, E., Grieser, B., and D. Kundert, 2008, A practical use of shale petrophysics for stimulation design optimization: Presented at the 2008 SPE Annual Technical Conference and Exhibition, SPE.

Rutledge, J. T., and Phillips, W. S., 2003, Hydraulic stimulation of natural fractures as revealed by induced microearthquakes, Carthage Cotton Valley gas field, east Texas: Geophysics, **68**, 441-452.

Warpinski, N. R., and S. L. Wolhart, 2004, Analysis and prediction of microseismicity induced by hydraulic fracturing: SPE Journal, **9**, 24-33.

Williams-Stroud, S., and P. M. Duncan, 2008, Microseismic mapping –the geological factor: E&P, **81**, 51-52.